Effects of low-frequency noise cross-correlations in coupled superconducting qubits

2008 New J. Phys. 10 115006

(http://iopscience.iop.org/1367-2630/10/11/115006)

New Journal of Physics
The open-access journal for physics

Effects of low-frequency noise cross-correlations in coupled superconducting qubits

A D'Arrigo[1], **A Mastellone, E Paladino and G Falci**
MATIS CNR-INFM, Catania and Dipartimento di Metodologie Fisiche e Chimiche per l'Ingegneria, Università di Catania, Viale Andrea Doria 6, 95125 Catania, Italy
E-mail: darrigo@femto.dmfci.unict.it

New Journal of Physics **10** (2008) 115006 (18pp)
Received 9 June 2008
Published 20 November 2008
Online at http://www.njp.org/
doi:10.1088/1367-2630/10/11/115006

Abstract. We study the effects of correlated low-frequency noise sources acting on a two-qubit gate in a fixed coupling scheme. A decoherence model for the spatial and cross-talk correlations is introduced. The efficiency inside the SWAP subspace is analyzed by combining analytic results based on the adiabatic approximation and numerical simulations. Results critically depend on amplitude of the low-frequency noise with respect to the qubits' coupling strength. Correlations between noise sources induce different qualitative behavior depending on the values of the above parameters. The possibility to reduce dephasing due to correlated low-frequency noise by a recalibration protocol is discussed.

[1] Author to whom any correspondence should be addressed.

Contents

1. Introduction

Solid-state nanodevices are at the forefront of present research toward the implementation of quantum networks for quantum computation and communication. The impressive development in device design and control tools achieved in recent years has by now to face intrinsic limitations due to material imperfections and fluctuations. The resulting noise presents a variety of material and device-dependent features, ranging from noise spectra showing narrow resonances at selected frequencies (sometimes resonant with the nanodevice relevant energy scales) to low-frequency high-amplitude noise, often displaying $1/f$ behavior. Modeling these fluctuations has naturally lead to overtake the ubiquitous effective bath description via harmonic models and/or the hypothesis of linear coupling to the device under investigation.

A typical example are background charge fluctuations which for more than 10 years have been known to strongly affect the performance of single-electron tunneling (SET) circuits [1]. Nowadays they represent the main limitation for any nanocircuit gate requiring highly reliable electrostatic control. This is clearly the case of charge [2] and charge-phase [3] superconducting qubits, but also of semiconducting spin qubits elecrostatically coupled to form a two-qubit gate [4].

The general belief is that background charge noise is due to the activity of random traps for single electrons in dielectric materials surrounding the island of SET devices or of superconducting nanocircuits. These traps may have different trapping energies and switching times, γ^{-1}. An ensemble of non-interacting traps with a uniform distribution of trapping energies and a $1/\gamma$ distribution of switching rates may originate the frequently observed $1/f$ noise [5]. Such a spectrum is indicative of numerous traps participating in the generation of the noise. On the other hand, some samples clearly produce a telegraph noise with random switching between a few states (with a magnitude of up to $0.1e$ in SET devices) [1, 6]. In addition, recent observations on superconducting qubits in different setups have suggested the possibility that a few impurities may entangle with the device [7, 8]. Such a variety of experimental facts may be consistently predicted by describing background charges as two-state systems whose dynamical behavior may turn from quantum mechanical to classical with increasing temperature and/or with increasing strength of their dissipative interaction with the

fluctuations of the surrounding local host [9]. Such a modelization clearly departs from the 'conventional' bosonic bath model and appropriately predicts the different protocol-dependent decay laws of the coherent dynamics observed in charge and charge-phase qubits [9]. Multiple frequencies in the qubit dynamics and dependence on the uncontrollable impurities' initial state at the beginning of measurement protocol are typical manifestations of non-gaussian character of background charge fluctuations [10].

In order to limit the effect on single-qubit gates of these material-specific fluctuations different strategies have been developed. Amongst the most successful is the design of nanocircuits operating at 'protected working points' insensitive to charge fluctuations of the lowest order in the noise strength [3]. Open- and closed-loop control protocols partly mutated from quantum optics and NMR [11], represent another promising route [12]–[14].

Presently, the effort of the scientific community working with Josephson qubits is to appropriately extend the above strategies to multiqubit architectures, the first step being to implement an efficient two-qubit gate. Different schemes to couple superconducting qubits have been proposed [15] and some experiments pointed out the possibility to realize the desired entangled dynamics [16]–[18]. However, achievement of the needed high fidelity is still an ambitious task. In addition to fluctuations experienced individually by each single-qubit gate, coupled qubits, being usually built on-chip, may suffer from correlated noise due to sources acting simultaneously on both sub-units. The effects on two-qubit gates of uncorrelated and correlated bosonic baths has been investigated [19].

As far as the effect of background charges, opinions about the probable location of traps are divided and observations depend to a certain extent on the specific sample and on the junction geometry. However, there is unambiguous evidence that fluctuating traps located in the insulating substrate contribute essentially to the total noise in SET devices [1, 20]. These traps are expected to induce similar fluctuations on the two islands built on the same substrate. On the other hand, fluctuating traps concentrated inside the oxide layer of the tunnel junctions, due to screening by the junction electrodes, are expected to act independently on the two qubits [1].

Fluctuating impurities acting simultaneously on coupled qubits represent a further unconventional noise source which solid-state nanodevices have to face [21]. This is the subject of the present paper. Specifically, we will introduce a model for correlated charge noise on interacting charge-phase qubits in a fixed capacitive coupling scheme. Relying on measurements on SET circuits of power spectra on the two transistors and of the cross-spectrum power density, we suppose a $1/f$ behavior for both the two-channel spectra and the cross-spectrum [1]. In addition, the cross-talk between the two qubits due to the capacitive coupling itself between the islands will be discussed. Our analysis is based on analytical results obtained within the adiabatic approximation for the $1/f$ noise and on the numerical solution of the stochastic Schrödinger equation. Solving the dynamics from short-to-intermediate timescales allows complete understanding of the effects of correlations. Our work extends the analysis of [21] which, being limited to the long-time behavior, misses relevant features occurring in the short-time domain. We find that usually correlations induce a faster decay of the coherent dynamics compared to the action of independent fluctuations. Nevertheless, under realistic values of low-frequency noise amplitude, increasing the degree of correlation may instead lead to longer decoherence times. Finally, the possibility of reducing the effects of low-frequency correlated noise via open-loop recalibration protocols is discussed.

The paper is organized as follows: in section 2, we introduce the setup consisting of two Cooper pair boxes (CPB) coupled by a capacitor. The cross-talk effect and the charge noise

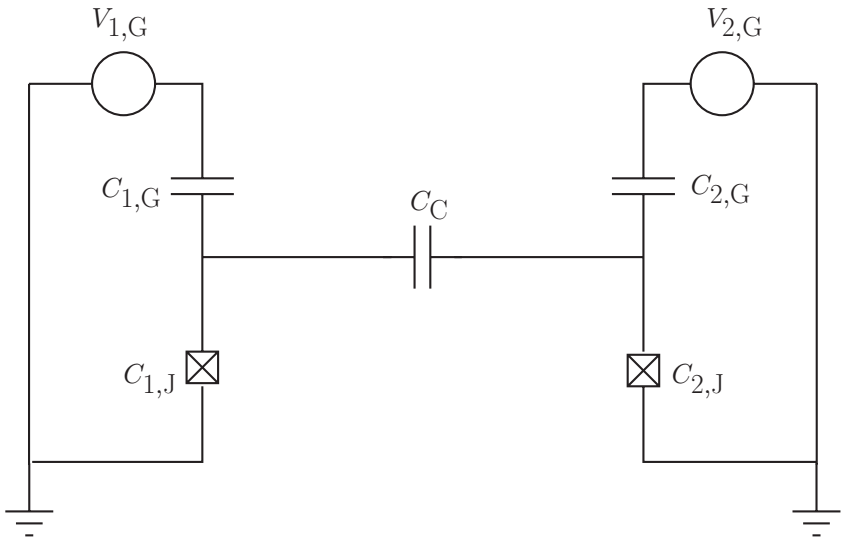

Figure 1. Two CPBs connected by a fixed capacitor.

sources responsible for correlations will be described and their correlation factor defined. In section 3, we present a possible model for correlated noise exhibiting $1/f$ power spectrum and cross-spectrum. In section 4, relevant dynamical quantities for a two-qubit gate are introduced and analytic/numerical methods are illustrated. Section 5 consists of our results for the entangled qubits dynamics in the presence of correlations. Conclusions are presented in section 6.

2. Coupled CPBs and noise correlations

In the fixed capacitive coupling scheme for charge [2] or charge-phase [3] qubits, the islands of two CPBs are connected through a capacitance [16, 17], as illustrated in figure 1. The system is described by the Hamiltonian

$$\mathcal{H}_0 = \sum_{\alpha\in\{1,2\}} \mathcal{H}_\alpha + E_{\mathrm{CC}}(\hat{q}_1 - q_{1,x})(\hat{q}_2 - q_{2,x}), \tag{1}$$

where each CPB is modeled by

$$\mathcal{H}_\alpha = [E_{\alpha,\mathrm{C}}(\hat{q}_\alpha - q_{\alpha,x})^2 + E_{\alpha,\mathrm{J}}\cos\hat{\varphi}_\alpha]. \tag{2}$$

$E_{\alpha,\mathrm{C}} = 2e^2/C_{\alpha,\Sigma}$ is the charging energy of the island belonging to CPB α, the total island capacitance $C_{\alpha,\Sigma} = C_{\alpha,\mathrm{G}} + C_{\alpha,\mathrm{J}}$ being the sum of the gate and junction capacitances. $q_{\alpha,x} = C_{\alpha,\mathrm{G}}V_{\alpha,\mathrm{G}}/(2e)$ is the corresponding dimensionless gate charge. Cooper pair tunneling across the Josephson junction α requires an energy $E_{\alpha,\mathrm{J}}$. $E_{\mathrm{CC}} = (2e)^2C_{\mathrm{T}}/(C_{1,\Sigma}C_{2,\Sigma})$ is the coupling energy, with $1/C_{\mathrm{T}} = 1/C_{\mathrm{C}} + 1/C_{1,\Sigma} + 1/C_{2,\Sigma}$ the total inverse capacitance of the device.

The dimensionless charge $\hat{q}$ and the phase $\hat{\varphi}$ of each box are conjugated variables, $[\hat{\varphi}, \hat{q}] = \mathrm{i}$. The system is subject to fluctuations of different origin. In part, they arise from the control circuitry and can be described by an effective impedance modeled by a conventional bosonic bath. Noise sources of microscopic origin are atomic defects located in the oxide of the tunnel junctions, leading to fluctuations of the Josephson energy and background charges acting like additional uncontrollable $q_{\alpha,x}$ sources. Devices based on the charge variable are

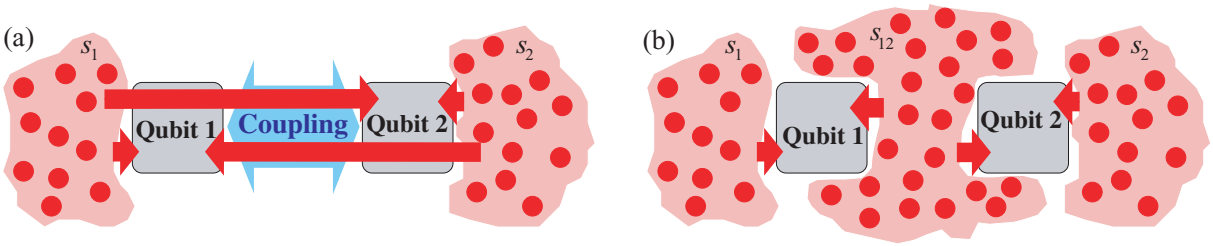

Figure 2. Pictorial representation of cross-talk (a) and spatial correlations (b). (a) The uncorrelated noise sources s_1 and s_2 act on coupled qubits: because of the coupling each qubit also suffers from the noise source directly acting on the other qubit. (b) Two non-interacting qubits in the presence of s_1, s_2 and of s_{12} that simultaneously act on both qubits. s_{12} may represent a set of impurities located in the insulating substrate. It generates a fluctuating interaction even in the absence of direct coupling between the two qubits.

particularly sensitive to background charge fluctuations. Usually they can be modeled as two-level fluctuators (TLF) inducing a bistable polarization of the superconducting island. A collection of TLF produces a noise whose spectral density approximately follows a $1/f$ law. They are responsible for the sensitive initial reduction of the amplitude of coherent oscillations in single-qubit gates observed when repeated measurements are performed [9, 12]. Fluctuations of polarization islands are expected to be a severe hindrance for coupled qubits gates based on the charge variable [22]. Low-frequency charge fluctuations lead to an additional stray contribution to the gate charge $q_{\alpha,x}$, which can be modeled by a random variable $\delta q_{\alpha,x}(t)$ leading to

$$\begin{aligned} \mathcal{H} &= \mathcal{H}_0 + \delta\mathcal{H}, \\ \delta\mathcal{H} &= -\hat{q}_1\left[2E_{1,\mathrm{C}}\delta q_{1,x}(t) + E_{\mathrm{CC}}\delta q_{2,\mathrm{x}}(t)\right] - \hat{q}_2\left[E_{\mathrm{CC}}\delta q_{1,x}(t) + 2E_{2,\mathrm{C}}\delta q_{2,x}(t)\right]. \end{aligned} \tag{3}$$

Note that the coupling capacitance induces a cross-talk between the two devices, i.e. fluctuations $\delta q_{1,x}(t)$ acting on $\hat{q}_2$ and vice-versa. As we already mentioned, background charges responsible for gate-charge fluctuations are spatially distributed in a device-dependent unpredictable way. Possibly they are partly located in the substrate, partly in the oxide layer covering all electrodes, partly in the oxide barriers of the tunnel junctions. Due to the shielding by the electrodes, impurities within tunnel junction α are expected to induce only gate-charge fluctuations $\delta q_{\alpha x}(\mathrm{t})$. On the other hand, random arrangement of noise sources in the bulk substrate produce correlations between gate-charge fluctuations to an extent depending on their precise location [1]. Pictorially, we may separate impurities into two ensembles $\{s_1, s_2\}$ and s_{12} influencing either each sub-unit or both islands, as illustrated in figure 2. The noise $\delta q_{\alpha,x}$ viewed by qubit α is due both to s_α and s_{12}. Correlations between $\delta q_{1,x}$ and $\delta q_{2,x}$ originate from set s_{12}, are termed *spatial correlations*.

In the above phenomenological description, we assume that $\delta q_{\alpha,x}(t)$ are stationary stochastic processes having zero average and the same variance $\bar{\sigma}^2$. We quantify the degree of spatial correlation between $\delta q_{1,x}$ and $\delta q_{2,x}$ via $\langle \delta q_{\alpha,x}(t)\delta q_{\beta,x}(t)\rangle = [\delta_{\alpha\beta} + \mu_{\mathrm{sp}}(1-\delta_{\alpha\beta})]\bar{\sigma}^2$. Evaluation of μ_{sp} would require a microscopic description of the device and it is expected to depend on the dimension of the boxes and on their relative distance, on the specific spatial distribution of impurities s_{12} and on the relative weights on $\delta q_{\alpha,x}(t)$ of fluctuations due to set s_{12} and s_α, as shown in [1].

Cross-talk due to coupling and spatial correlations enters the overall noise X_α felt by each sub-unit

$$X_1(t) = 2E_{1,\mathrm{C}}\,\delta q_{1,x}(t) + E_{\mathrm{CC}}\,\delta q_{2,x}(t), \tag{4}$$

$$X_2(t) = E_{\mathrm{CC}}\,\delta q_{1,x}(t) + 2E_{2,\mathrm{C}}\,\delta q_{2,x}(t). \tag{5}$$

The amount of correlation between X_1 and X_2 may be quantified by a correlation coefficient, which is defined for general stochastic processes ξ_1 and ξ_2 as [23]

$$\mu = \frac{\left\langle \left[\xi_1(t) - \bar{\xi}_1\right]\left[\xi_2(t) - \bar{\xi}_2\right]\right\rangle}{\sqrt{\left\langle \left[\xi_1(t) - \bar{\xi}_1\right]^2\right\rangle \left\langle \left[\xi_2(t) - \bar{\xi}_2\right]^2\right\rangle}}, \tag{6}$$

where $\langle\cdot\rangle$ indicates the ensemble average, and $\bar{\xi}_i \equiv \langle \xi_i(t)\rangle$. From (4) and (5) we obtain

$$\begin{aligned}\langle X_\alpha^2\rangle &= (4E_{\alpha,\mathrm{C}}^2 + E_{\mathrm{CC}}^2 + 4\mu_{\mathrm{sp}}E_{\alpha,\mathrm{C}}E_{\mathrm{CC}})\overline{\sigma}^2,\\ \langle X_1X_2\rangle &= [2E_{\mathrm{CC}}(E_{1,\mathrm{C}} + E_{2,\mathrm{C}}) + \mu_{\mathrm{sp}}(4E_{1,\mathrm{C}}E_{2,\mathrm{C}} + E_{\mathrm{CC}}^2)]\overline{\sigma}^2;\end{aligned}$$

thus, the correlation coefficient of X_1 and X_2 reads

$$\mu = \frac{2E_{\mathrm{CC}}(E_{1,\mathrm{C}} + E_{2,\mathrm{C}}) + \mu_{\mathrm{sp}}(4E_{1,\mathrm{C}}E_{2,\mathrm{C}} + E_{\mathrm{CC}}^2)}{\sqrt{\left(4E_{1,\mathrm{C}}^2 + E_{\mathrm{CC}}^2 + 4\mu_{\mathrm{sp}}E_{1,\mathrm{C}}E_{\mathrm{CC}}\right)\left(4E_{2,\mathrm{C}}^2 + E_{\mathrm{CC}}^2 + 4\mu_{\mathrm{sp}}E_{2,\mathrm{C}}E_{\mathrm{CC}}\right)}}. \tag{7}$$

In the absence of spatial correlations, $\delta q_{\alpha,x}$ are independent and only the effect of cross-talk is left. The correlation coefficient in this case is reduced to

$$\mu_{\mathrm{ct}} = \frac{2E_{\mathrm{CC}}(E_{1,\mathrm{C}} + E_{2,\mathrm{C}})}{\sqrt{\left(4E_{1,\mathrm{C}}^2 + E_{\mathrm{CC}}^2\right)\left(4E_{2,\mathrm{C}}^2 + E_{\mathrm{CC}}^2\right)}} \simeq \frac{4E_{\mathrm{C}}E_{\mathrm{CC}}}{\left(4E_{\mathrm{C}}^2 + E_{\mathrm{CC}}^2\right)}. \tag{8}$$

In the last approximation we have supposed $E_{\alpha,\mathrm{C}} \simeq E_{\mathrm{C}}$, within manufacturing tolerances. For typical values of parameters for charge qubits $E_{\mathrm{C}} \gg E_{\mathrm{CC}}$, thus $\mu_{\mathrm{ct}} \simeq E_{\mathrm{CC}}/E_{\mathrm{C}}$, giving values between 0.015 [22] and 0.12 [17]. Clearly, larger values of the coupling strength E_{CC}, desirable to produce faster two-qubit gates, would also lead to higher cross-talk correlations μ_{ct}. In general, the correlation coefficient (7) for $E_{\alpha,\mathrm{C}} \simeq E_{\mathrm{C}}$ is approximately given by

$$\mu \simeq \frac{4E_{\mathrm{C}}E_{\mathrm{CC}} + \mu_{\mathrm{sp}}(4E_{\mathrm{C}}^2 + E_{\mathrm{CC}}^2)}{4E_{\mathrm{C}}^2 + E_{\mathrm{CC}}^2 + 4\mu_{\mathrm{sp}}E_{\mathrm{C}}E_{\mathrm{CC}}} = \frac{\mu_{\mathrm{ct}} + \mu_{\mathrm{sp}}}{1 + \mu_{\mathrm{ct}}\mu_{\mathrm{sp}}}, \tag{9}$$

where we used (8). Strong correlations between X_1 and X_2, $\mu \approx 1$, may originate either from large cross-talk or from large spatial correlations. For instance by engineering device design [24] it could be possible to get $\mu_{\mathrm{ct}} \simeq 1$ implying $\mu \simeq 1$. On the other hand, in the presence of a low level of correlations $\mu_{\mathrm{sp}}\mu_{\mathrm{ct}} \ll 1$, equation (9) is simplified to $\mu \simeq \mu_{\mathrm{sp}} + \mu_{\mathrm{ct}}$.

In general, (7) gives the overall amount of correlation between fluctuations affecting the two CPBs. In the following, we will not specify the physical mechanism responsible for these correlations. We will simply suppose the existence of a degree of correlation between the fluctuations X_1 and X_2 quantified by the coefficient μ.

3. Charge noise power spectra and cross-spectrum

Measurements of charge noise due to background charge fluctuations in SET devices [1] have revealed a $1/f$ behavior at low frequencies (measurements extend down to about 1 Hz), with a roll-off frequency of 100–1000 Hz. Two SET whose islands are positioned about 100 nm apart show similar $1/f$ behavior for the cross-spectrum (defined later by (11)) indicating correlations between fluctuations affecting both islands. Similarly, measurements of charge noise in charge-phase [12] qubits show a $1/f$ behavior for $f < 100$ kHz whose amplitude depends on temperature, on junction size and on screening of the island by electrodes. Echo experiments suggest that $1/f$ noise extends up to 1 MHz. In this setup, charge noise at higher frequencies (up to 10 MHz) is due to driving and readout subcircuits and it is characterized by white spectrum. Measurements of energy relaxation processes in charge qubits have suggested that charged impurities may also be responsible for ohmic noise at gigahertz frequencies [25]. To our knowledge, measurements of cross-spectrum on this class of nanodevices have not been reported in the literature. It is however expected that, similarly to SET devices, correlations between fluctuations acting on superconducting islands of the two on-chip CPBs display $1/f$ cross-spectrum at low frequencies.

Our goal is to introduce a model for the fluctuations $X_1(t)$ and $X_2(t)$ such that both power spectra and cross-spectrum

$$S_{X_\alpha}(\omega) = \int_{-\infty}^{+\infty} \mathrm{d}\tau\, \mathrm{e}^{-\mathrm{i}\omega\tau} \left[\langle X_\alpha(t+\tau) X_\alpha(t)\rangle - \bar{X}_\alpha^2 \right] \tag{10}$$

$$S_{X_1X_2}(\omega) = \int_{-\infty}^{+\infty} \mathrm{d}\tau\, \mathrm{e}^{-\mathrm{i}\omega\tau} \left[\langle X_1(t+\tau) X_2(t)\rangle - \bar{X}_1\bar{X}_2 \right] \tag{11}$$

display similar $1/f$ behavior at low frequencies and are characterized by a finite correlation coefficient defined by (6). To this end, we introduce two *independent* stationary stochastic processes, $n_1(t)$ and $n_2(t)$ with the same average and characterized by the same autocovariance function and spectrum [23]

$$\begin{aligned} C_{n_\alpha n_\alpha}(\tau) &= \langle n_\alpha(t+\tau) n_\alpha(t)\rangle - \bar{n}_\alpha^2 \equiv C(\tau), \\ S_{n_\alpha n_\alpha}(\omega) &= \int_{-\infty}^{+\infty} \mathrm{d}\tau\, \mathrm{e}^{-\mathrm{i}\omega\tau} C(\tau) \equiv S(\omega). \end{aligned} \tag{12}$$

The processes $X_1(t)$ and $X_2(t)$, defined as linear combinations of $n_1(t)$ and $n_2(t)$,

$$\begin{aligned} X_1(t) &= \sqrt{1-\eta}\, n_1(t) + \sqrt{\eta}\, n_2(t) \\ X_2(t) &= \sqrt{\eta}\, n_1(t) + \sqrt{1-\eta}\, n_2(t) \end{aligned} \tag{13}$$

with $\eta \in [0, \frac{1}{2}]$ are correlated and their correlation coefficient reads

$$\mu = 2\sqrt{\eta(1-\eta)}. \tag{14}$$

Thus, μ is a monotonic function of $\eta \in [0, \frac{1}{2}]$ ranging in the interval [0,1], if $\eta = 0$, X_1 and X_2 reduce respectively to the uncorrelated processes n_1 and n_2, and $\mu = 0$. Instead when $\eta = \frac{1}{2}$, the correlation factor reaches its maximum value $\mu = 1$. In this case, X_1 and X_2 are reduced to the same process

$$\mu = 1 \quad \Rightarrow \quad X_1(t) = X_2(t) = \frac{1}{\sqrt{2}}[n_1(t) + n_2(t)]. \tag{15}$$

The autocovariance functions of $X_1(t)$ and $X_2(t)$ are identical and read

$$C_{X_\alpha X_\alpha}(\tau) = \langle X_\alpha(t+\tau)X_\alpha(t)\rangle - \bar{X}_\alpha^2 = (1-\eta)\, C_{n_1 n_1} + \eta\, C_{n_2 n_2} = C(\tau)\,, \tag{16}$$

therefore X_1 and X_2 have the same variance σ^2, and equal power spectra $S_{X_1}(\omega) = S_{X_1}(\omega) = S(\omega)$ given by (12). This simple model for correlated noise allows, by changing the arbitrary parameter η, to modulate the correlation coefficient between X_1 and X_2 from 0 to 1, maintaining the desired spectrum $S(\omega)$ for both processes. It is worth noticing that the first-order statistics of X_1 and X_2 depends on η: $\bar{X}_1 = \bar{X}_2 = \bar{n}(\sqrt{1-\eta} + \sqrt{\eta})$. To avoid this dependence we set $\overline{n} = 0$, implying vanishing average values for X_1 and X_2. The correlation factor enters the cross-covariance and the cross-spectrum of X_1 and X_2 [23]

$$C_{X_1 X_2}(\tau) = \langle X_1(t+\tau)X_2(t)\rangle - \overline{X}_1\overline{X}_2 = \mu\, C(\tau), \tag{17}$$

$$S_{X_1 X_2}(\omega) = \int_{-\infty}^{+\infty} \mathrm{d}\tau\, \mathrm{e}^{-\mathrm{i}\omega\tau}\, C_{X_1 X_2}(\tau) = \mu\, S(\omega). \tag{18}$$

It can therefore be detected by spectral analysis via [26]

$$\frac{S_{X_1 X_2}(\omega)}{\sqrt{S_{X_1}(\omega) S_{X_1}(\omega)}} = \mu. \tag{19}$$

By measuring power spectra and cross-spectrum of voltage fluctuations across each SET in the frequency range 1–10 Hz, Zorin *et al* [1] estimated according to (19) the correlation coefficient $\mu = 0.15 \pm 0.05$.

In order to obtain a $1/f$ spectrum for processes $X_\alpha(t)$, we adopt a commonly employed model which consists of an ensemble of independent TLF. Each fluctuator incoherently switches between two metastable levels, with a rate γ_k, producing a random signal $\xi_k(t)$. This signal has a Lorentzian power spectrum, $S_{\xi_k}(\omega) = \frac{1}{2} v_k^2 \gamma_k/(\gamma_k^2 + \omega^2)$, v_k being the difference between the values assumed by $\xi_k(t)$. When the switching rates γ_k are distributed according to $P(\gamma) \propto 1/\gamma$ in $[\gamma_\mathrm{m}, \gamma_\mathrm{M}]$, the overall noise obtained by summing all TLF contributions displays $1/\omega$ behavior in $[\gamma_\mathrm{m}, \gamma_\mathrm{M}]$ [5]

$$\xi = \sum_k \xi_k(t) \quad \Rightarrow \quad S_\xi(\omega) = \sum_{k=1}^{N_\mathrm{TLF}} \frac{v_k^2 \gamma_k}{2(\gamma_k^2 + \omega^2)} \simeq \frac{\mathcal{A}}{\omega}, \tag{20}$$

where $\mathcal{A} = \pi \langle v^2\rangle N_\mathrm{TLF}/[4\ln(\gamma_\mathrm{M}/\gamma_\mathrm{m})]$ and N_TLF is the total number of fluctuators. If the independent random processes $n_1(t)$ and $n_2(t)$ are generated as a sum of such an ensemble of TLFs, the spectrum of each $n_\alpha(t)$ will be $1/f$ in $[\gamma_\mathrm{m}, \gamma_\mathrm{M}]$ and will have variance $\sigma^2 = \frac{1}{2\pi}\int \mathrm{d}\omega\, S(\omega) = \frac{1}{4} N_\mathrm{TLF}\langle v^2\rangle$. The $1/f$-correlated stochastic processes $X_1(t)$ and $X_2(t)$ are obtained from (13), once the phenomenological correlation factor μ is fixed.

4. Two-qubit gate and relevant dynamical quantities

At sufficiently low temperatures each CPB may operate as an effective two-state system, the coupled boxes implementing a two-qubit gate. In the fixed coupling scheme, the interaction is switched on by individually manipulating each qubit to enforce mutual resonance conditions [16, 17]. This allows the realization of elementary two-qubit operations. We denote the lowest eigenstates of each CPB as $\{|+\rangle_\alpha, |-\rangle_\alpha\}$, with splitting depending on the control parameter $q_{\alpha,x}$, $\Omega_\alpha(q_{\alpha,x})$. By operating at the so-called 'charge-protected point',

Table 1. Eigenvalues and eigenvectors of $\mathcal{H}_0$. Here, $\sin\varphi = g/(2\sqrt{1+g^2/4})$ and $\cos\varphi = -1/\sqrt{1+g^2/4}$.

i	$\lambda_i^{(0)}$	$\|i\rangle$
0	$-\sqrt{1+g^2/4}$	$[-(\sin\varphi/2)\|++\rangle + (\cos\varphi/2)\|--\rangle]$
1	$-g/2$	$(-\|+-\rangle + \|-+\rangle)/\sqrt{2}$
2	$g/2$	$(\|+-\rangle + \|-+\rangle)/\sqrt{2}$
3	$\sqrt{1+g^2/4}$	$[(\cos\varphi/2)\|++\rangle + (\sin\varphi/2)\|--\rangle]$

$q_{\alpha,x} = 1/2$, the system is insensitive to charge fluctuations at lowest order, meaning that $\mathrm{d}\Omega_\alpha(q_{\alpha,x})/\mathrm{d}q_{\alpha,x}|_{q_{\alpha,x}=0.5} = 0$ [3]. In a pseudo-spin description, in the eigenstate basis charge fluctuations are off-diagonal at this working point. Therefore, projecting the coupled boxes Hamiltonian (2) into the computational subspace $\{|i\rangle_1 \otimes |j\rangle_2\} - i, j \in \{+, -\}$ we get,

$$\tilde{\mathcal{H}} = \tilde{\mathcal{H}}_0 + \delta\tilde{\mathcal{H}}, \tag{21}$$

$$\tilde{\mathcal{H}}_0 = -\frac{\Omega}{2}\sigma_3^{(1)} \otimes \mathbb{I}^{(2)} - \frac{\Omega}{2}\mathbb{I}^{(1)} \otimes \sigma_3^{(2)} + \frac{\tilde{E}_{\mathrm{CC}}}{2}\sigma_1^{(1)} \otimes \sigma_1^{(2)}, \tag{22}$$

$$\delta\tilde{\mathcal{H}} = -\frac{\tilde{X}_1}{2}\sigma_1^{(1)} \otimes \mathbb{I}^{(2)} - \frac{\tilde{X}_2}{2}\mathbb{I}^{(1)} \otimes \sigma_1^{(2)}, \tag{23}$$

where we assume the two qubits are tuned at the same Bohr splitting Ω, whose typical value is of the order $10^{11}\,\mathrm{rad\,s^{-1}}$. Here, $\tilde{E}_{\mathrm{CC}} = 2E_{\mathrm{CC}}\, q_{1,+-}\, q_{2,+-}$ and $\tilde{X}_\alpha = 2X_\alpha\, q_{\alpha,+-}$, being $q_{\alpha,+-} = \langle +|_\alpha \hat{q}_\alpha |-\rangle_\alpha$.

We remark that this symmetric configuration is hardly reachable in practice by fabrication accuracy only. In the charge-phase implementation [3] this can be achieved thanks to the characteristic two-port design. The quantization is in fact based on a split CPB connected to a large measurement Josephson junction, the phase across it, δ, representing an additional control knob. The device presents a 'doubly' protected point at $q_x = 1/2$ and $\delta = 0$, which is a saddle point of the single-qubit energy splitting versus external parameters. In the two-qubit setup resonance is achieved by slightly displacing one of the qubits from the phase-protected point, but maintaining both qubits at the charge-protected point. This setup is therefore expected to be sensitive also to phase fluctuations and this topic will be addressed elsewhere [27].

The setup described by (21) may in principle implement an iSWAP gate. This is easily illustrated in its eigenstate basis, reported in table 1 in terms of the dimensionless coupling strength $g = \tilde{E}_{\mathrm{CC}}\,\Omega^{-1}$. In the absence of fluctuations, the two-qubit Hilbert space is factorized in two subspaces spanned by pairs of computational states. In particular, the system prepared in the state $|+-\rangle$, freely evolves inside the subspace spanned by $\{|+-\rangle, |-+\rangle\}$, reaching the entangled state $(|+-\rangle + \mathrm{i}|-+\rangle)/\sqrt{2}$ at time $\bar{\tau} = \bar{t}\Omega = \pi/2g$. States $\{|1\rangle, |2\rangle\}$ generate the so-called SWAP subspace, whereas we refer to the Z subspace as the one spanned by $\{|0\rangle, |3\rangle\}$ [27].

A numerical analysis has shown that for typical values of parameters in charge-phase qubits, the SWAP-eigenvalues are more stable than single-qubit splitting with respect to uncorrelated gate-charge fluctuations [28]. As a consequence, for sufficiently small-amplitude, low-frequency charge fluctuations the decay time for entangled states in the SWAP subspace is

expected to be longer than the single-qubit dephasing time [28]. In the following, we analyze how low-frequency correlations between charge noise felt by each qubit may influence the dynamics in the SWAP subspace.

4.1. Relevant dynamical quantities

In the presence of low-frequency fluctuations the calibration of the device is unstable. As a result, the quantum dynamics of the interacting qubits will depend on the measurement protocol, as already observed for single-qubit gates. Ideal quantum protocols assume measurements of individual members of an ensemble of identical (meaning that the preparation is controlled) evolutions, defocusing occurring during time evolution. In practice, for solid-state nanodevices several samples are collected during an overall measurement time $t_{\rm m}$. Lack of control of the environment preparation determines defocusing of the signal, analogous to inhomogeneous broadening in NMR. The considerable initial reduction of the amplitude of the coherent oscillations of single-qubit gates affected by $1/f$ charge noise is due precisely to this effect [9, 12]. On the other hand, the effect of low-frequency noise on relaxation processes is negligible. Thus, the system dynamics can be treated in the adiabatic approximation for the low-frequency charge fluctuations. Under this approximation scheme, populations of the system eigenstates do not evolve. The relevant dynamical quantities are therefore the off-diagonal elements of the system density matrix in the same basis.

The efficiency of the iSWAP protocol in the presence of $1/f$ spectra on both qubits and $1/f$ cross-spectrum can therefore be extracted by evaluating a single dynamical quantity, the coherence between the eigenstates of the SWAP subspace. The two-qubit density matrix in the presence of the dimensionless classical stochastic processes $x_i(t) = X_i(t)/\Omega$ generally reads

$$\rho(\tau) = \int \mathcal{D}[x_1(\tau')]\mathcal{D}[x_2(\tau')]P[x_1(\tau'), x_2(\tau')]\rho[\tau|x_1(\tau'), x_2(\tau')], \tag{24}$$

where $\rho[\tau|x_1(\tau'), x_2(\tau')]$ is the system density matrix calculated for a given realization $\{x_1(\tau'), x_2(\tau')\}$. The integration is over all possible realizations weighted by the probability density $P[x_1(\tau), x_2(\tau)]$.

We solved equation (24) numerically by generating the independent random processes $n_1(\tau)$ and $n_2(\tau)$ and from them the correlated processes $x_1(t)$ and $x_2(t)$, as illustrated in section 3. The Schrödinger equation related to the Hamiltonian (21) is numerically solved by a fourth-order Runge–Kutta algorithm [29], calculating the system dynamics $\rho[\tau|x_1(\tau), x_2(\tau)]$. These operations are repeated to perform an average of $\rho[\tau|x_1(\tau), x_2(\tau)]$ over many ($\geqslant 10^4$) realizations of the stochastic processes. Numerical simulations confirm that in the presence of low-frequency noise (with $\gamma_{\rm M} < 10^{-2}\,\Omega$) transitions between the SWAP and Z subspaces can be neglected. This further legitimizes focusing on the coherence in the SWAP subspace which reads as

$$\begin{aligned}\langle 1|\rho(\tau)|2\rangle &\equiv \rho_{12}(\tau)\\ &= \rho_{12}(0)\mathrm{e}^{-\mathrm{i}g\tau}\mathrm{e}^{-\mathrm{i}\Phi(\tau)}\\ &= \rho_{12}(0)\cdot\int\mathcal{D}[x_1(\tau')]\mathcal{D}[x_2(\tau')]P[x_1(\tau'), x_2(\tau')]\exp\left[\mathrm{i}\int_0^{\tau'}\mathrm{d}\tau''\omega_{12}[x_1(\tau''), x_2(\tau'')]\right],\end{aligned} \tag{25}$$

where $\omega_{12}[x_1(\tau''), x_2(\tau'')]$ gives the noise-renormalized splitting between states $|1\rangle$ and $|2\rangle$. The imaginary part of $\Phi(\tau)$ describes the decay of the entangled dynamics in the presence of adiabatic correlated noise. Further insight can be obtained by approximating (25) to include the dominant inhomogeneous broadening effect. This is performed by applying the static path approximation (SPA), $x_\alpha(t) \equiv x_\alpha$, which accounts for the lack of control of the device calibration via a statistical distributed gate charge at each run of the measurement protocol. In the SPA the coherence (25) reduces to the evaluation of an ordinary two-variable integral

$$\rho_{12}(\tau) = \rho_{12}(0) \int \mathrm{d}x_1\, \mathrm{d}x_2\, P(x_1, x_2)\, \exp\left[\mathrm{i}\tau\omega_{12}(x_1, x_2)\right], \tag{26}$$

where $P(x_1, x_2)$ is the joint probability density function of the random variables x_1 and x_2 [23]. In the following, we will use the notation $\langle f(x_1, x_2)\rangle$ to indicate $\int \mathrm{d}x_1\, \mathrm{d}x_2\, P(x_1, x_2)\, f(x_1, x_2)$.

In the following section, we will analytically evaluate the coherence in the SWAP subspace within the SPA in selected parameter regimes where numerical simulations have confirmed its accuracy. A numerical analysis will be performed to estimate the decay of entanglement under more general conditions.

5. Dephasing in the SWAP subspace: effects of correlations

The average in (26) is conveniently evaluated by performing the change of variables (13). In fact, since the independent random processes $n_1(t)$ and $n_2(t)$ are generated from a large number of TLFs, their initial values n_α are Gaussian distributed

$$P(n_\alpha) = \frac{1}{\sqrt{2\pi}\sigma} \exp[-n_\alpha^2/(2\sigma_{n_\alpha}^2)]. \tag{27}$$

Clearly, x_1 and x_2 are two correlated Gaussian variables whose joint probability density function is (for $|\mu| < 1$) [23]:

$$P(x_1, x_2) = \frac{1}{2\pi\sigma^2\sqrt{1-\mu^2}} \exp\left[-\frac{1}{2\sigma^2(1-\mu^2)}\left(x_1^2 + x_2^2 - 2\mu x_1 x_2\right)\right]. \tag{28}$$

The effective splitting in the SWAP subspace in the presence of charge fluctuations entering the average (26) may be evaluated by exact diagonalization of the Hamiltonian (21). The solution of the resulting fourth-order polynomial is rather lengthy, so we have not reported it here. Relevant features can be extracted by expanding the splitting up to the fourth order in x_α and keeping the dominant terms in the coupling strength g [27]

$$\omega_{12}(x_1, x_2) \approx g - \frac{g}{2}\left(x_1^2 + x_2^2\right) + \frac{1}{8g}(x_1^2 - x_2^2)^2 \equiv g + \delta\omega_{12}(x_1, x_2). \tag{29}$$

This expansion suggests that the system behavior depends on the relative weight of the amplitude of the noise, measured in the SPA by the standard deviation σ entering (28), and the strength of the interaction between the qubits, g. In the following, we consider separately the two regimes of 'weak' and 'strong' amplitude noise, $\sigma < g$ and $\sigma > g$, respectively. We remark that the nonmonotonic dependence of the splitting on x_α may lead to almost degeneracy between the renormalized levels of the SWAP subspace. This effect may be relevant when the interplay of low- and high-frequency components is considered [27].

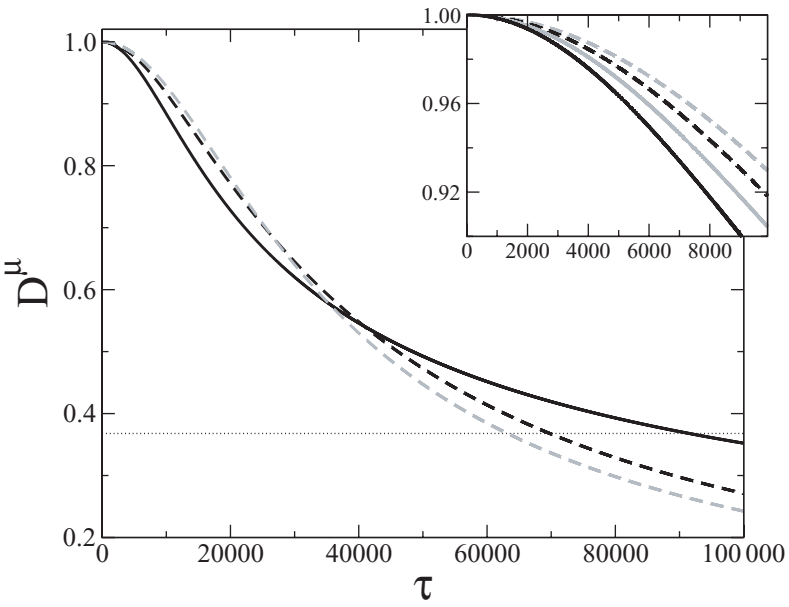

Figure 3. Dephasing factor given by (31) for different values of the correlation coefficient μ for 'weak' amplitude noise, $\sigma = 0.02 < g = 0.1$. The dashed gray curve refers to the uncorrelated case $\mu = 0$, the dashed black to $\mu = 0.50$, the thick black refers to $\mu = 1.00$. The crossing of each curve with the dotted horizontal line at e^{-1} identifies the estimated dephasing time relative to each value of μ, $\tau_2(\mu)$. Intersections with the curve corresponding to uncorrelated noise $(\mu = 0)$ identifies the time $\tau^*(\mu) < \tau_2$. Inset: enlargement for short times. The thick gray line corresponds to $\mu = 0.75$. The validity of the SPA approximation has been checked against numerical simulations for stochastic processes exhibiting a $1/f$ power spectrum in a range $[\gamma_m, \gamma_M] = [1, 10^6]$ s^{-1} (not shown).

Weak amplitude noise $\sigma \ll g$. In this regime, (29) can be approximated by keeping terms up to second order in σ so that $\delta\omega_{12}^{w}(x_1, x_2) = -\frac{g}{2}(x_1^2 + x_2^2)$. The average

$$\rho_{12}(\tau) = \rho_{12}(0)\, e^{ig\tau} \langle \exp(-i\tau\delta\omega_{12}^{w}) \rangle \tag{30}$$

can be easily evaluated and leads, for the dephasing factor

$$D_{12}^{\mu}(\tau) = \left| \frac{\rho_{12}(\tau)}{\rho_{12}(0)} \right| = \left[1 + (g\sigma^2(1-\mu)\tau)^2\right]^{-1/4} \times \left[1 + (g\sigma^2(1+\mu)\tau)^2\right]^{-1/4}. \tag{31}$$

The dephasing factor factorizes into two contributions having the form of the decay of the single-qubit coherence at protected point in the SPA [9] with standard deviations $\sigma\sqrt{1 \pm \mu}$. An analogous result has been found in [21]. Equation (31) is shown in figure 3 for different values of the correlation coefficient μ. For comparison, the curve corresponding to independent noise sources acting on the two qubits is also reported, $D_{12}^{\mu=0}(\tau) = [1 + (g\sigma^2\tau)^2]^{-1/2}$. Interestingly, at short times increasing the correlation coefficient induces a faster reduction of the amplitude of coherent oscillations in the SWAP subspace. This behavior crosses over to a regime where instead of increasing, the correlation coefficient slows down dephasing. This occurs during

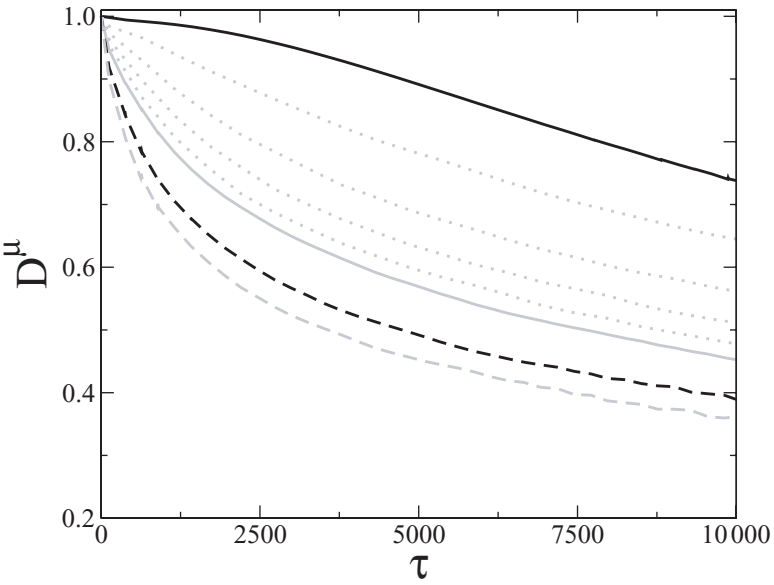

Figure 4. Dephasing factor $D_{12}^{\mu}(\tau)$ for strong amplitude noise, $g = 0.01 < \sigma = 0.08$. Curves correspond to different values of the correlation coefficient, from bottom to top $\mu \in \{0, 0.50, 0.75, 0.8, 0.85, 0.90, 0.95, 1.00\}$. Correlations improve the system performance despite the large noise amplitude.

times larger than τ^* identified by the condition $D_{12}^{\mu}(\tau^*) = D_{12}^{0}(\tau^*)$, which gives $\tau^*(\mu) = 1/(g\sigma^2\sqrt{1-\mu^2/2})$. The crossover takes place at times shorter than the dephasing time where $D_{12}^{\mu}(\tau_2) = \mathrm{e}^{-1}$

$$\tau_2(\mu) = \frac{\sqrt{-(1+\mu^2)+\sqrt{(1+\mu^2)^2+(e^4-1)(1-\mu^2)^2}}}{g\sigma^2(1-\mu^2)} > \tau^*(\mu)\,. \tag{32}$$

We remark that, for quantum computing purposes, it is crucial to understand the behavior at times shorter than the dephasing time. For instance, fault-tolerant quantum computation [30, 31], i.e. implementing reliable quantum operations even in the presence of errors, requires errors to be maintained below a small threshold (typically $\epsilon_{\mathrm{th}} \sim 10^{-4}$–$10^{-6}$). The error of the iSWAP gate under investigation may be simply estimated as (in the adiabatic approximation)

$$\epsilon = 1 - \langle\psi|\rho(\tau)|\psi\rangle = 1 - \tfrac{1}{2}D_{12}^{\mu}(\tau) \tag{33}$$

$|\psi\rangle$ being the iSWAP target state. This leads, at the dephasing time τ_2, to an error of about 0.8. The correlation coefficient dependence of the dephasing time τ_2 [21] does not reveal relevant features of the iSWAP gate operation occurring at initial timescales.

Strong amplitude noise $\sigma \gg g$. For larger amplitudes of the noise, the dephasing factor displays completely different behavior. Numerical results are illustrated in figure 4. In this case increasing the correlation coefficient systematically *reduces* dephasing. In particular, the limiting case $\mu = 1$, where the same noise simultaneously acts on both qubits, turns out to be relatively weakly affected by the low-frequency noise, despite its large amplitude.

The short-time behavior and its dependence on the correlation coefficient for weak and strong amplitude noises may be explained considering the renormalized splitting dependence

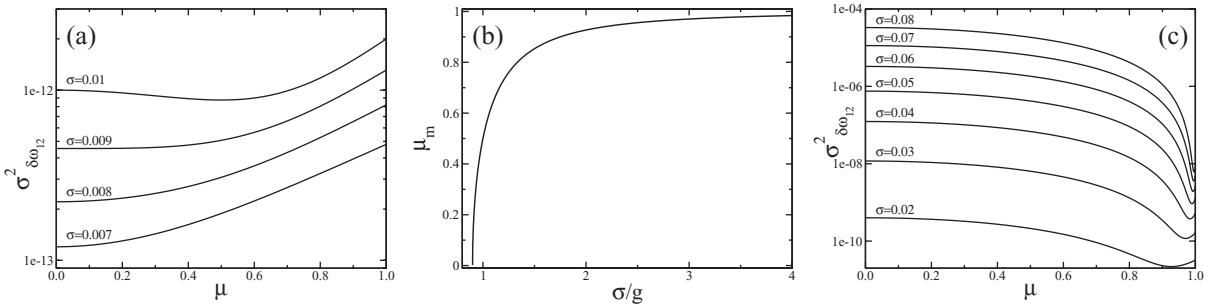

Figure 5. (a) Variance (35) as a function μ, for small amplitude noise $\sigma \lesssim g$. (b) Correlation coefficient where the variance attains its minimum, as a function of the ratio σ/g. For $\sigma \geqslant 4g$, it is $\mu_{\rm m} \simeq 1$. (c) Equation (35) as a function of μ for $\sigma \gg g$. $\sigma^2_{\delta\omega_{12}}$ decreases by different orders of magnitudes when $\mu \geqslant 0.8$. In (a) and (c) $g = 0.01$.

on the noise variables x_α. The level splitting itself in fact can be viewed as a random variable, with standard deviation $\sigma_{\delta\omega_{12}} = \sqrt{\langle\delta\omega_{12}^2\rangle - \langle\delta\omega_{12}\rangle^2}$. The short times Gaussian approximation for the dephasing factor gives

$$D_{12}^{\mu}(\tau) \simeq 1 - \tfrac{1}{2}\sigma^2_{\delta\omega_{12}}\tau^2, \tag{34}$$

thus, at times short enough that $\sigma_{\delta\omega_{12}}\tau < 1$ (for data in figure 3, $\tau < 10^4$), a larger deviation $\sigma_{\delta\omega_{12}}$ induces a larger dephasing, i.e. a smaller value for $D_{12}^{\mu}(\tau)$. The variance of $\delta\omega_{12}$ reads (see appendix for details)

$$\sigma^2_{\delta\omega_{12}} = \frac{\sigma^4}{g^2}\left\{\left[(g^2-\sigma^2)^2+\sigma^4\right] + \mu^2\left[(g^2+\sigma^2)^2 - 5\sigma^4\right] + 2\mu^4\sigma^4\right\}. \tag{35}$$

For $\sigma < g$, it reduces approximately to $\sigma^2_{\delta\omega_{12}{}^{\rm w}} = g^2\sigma^4(1+\mu^2)$, monotonically increasing with μ, as shown in figure 5(a). This explains the stronger dephasing observed for small amplitude noise at short times. On the other hand, for $\sigma > g$, $\sigma^2_{\delta\omega_{12}}$ is nonmonotonic with a minimum at $\mu_{\rm m} = [1 - \frac{1}{2}(\sigma/g)^{-2} - \frac{1}{4}(\sigma/g)^{-4}]^{1/2}$, which rapidly approaches 1 (figure 5(b)). Thus, for $\mu \to 1$ the splitting variance rapidly reaches its minimum value, implying small dephasing at short times even for large noise amplitudes, $\sigma \geqslant 4g$.

5.1. Effects of higher frequencies and recalibration protocol

We now consider the effect of correlated $1/f$ noise extending to higher frequencies maintaining the adiabaticity condition with respect to the qubit splitting Ω, i.e. we simulate fluctuations leading to $1/f$ spectrum up to the cut-off frequency $\gamma_{\rm M} = 10^9\,{\rm s}^{-1}$. The resulting dephasing in this case, in addition to the inhomogeneous broadening mechanism, also originates from the dynamics of the fluctuators during the time evolution. The dependence of the dephasing factor on the correlation coefficient μ has the same characteristics observed in the presence of low-frequency components only. The system still displays different behavior depending on σ being smaller or larger than g. This is illustrated in figures 6(a) and 7(a). In particular, the very low dephasing already observed when the qubits are affected by the same environment ($\mu = 1$), persists also in the presence of high-frequency noise components (figure 7(a)).

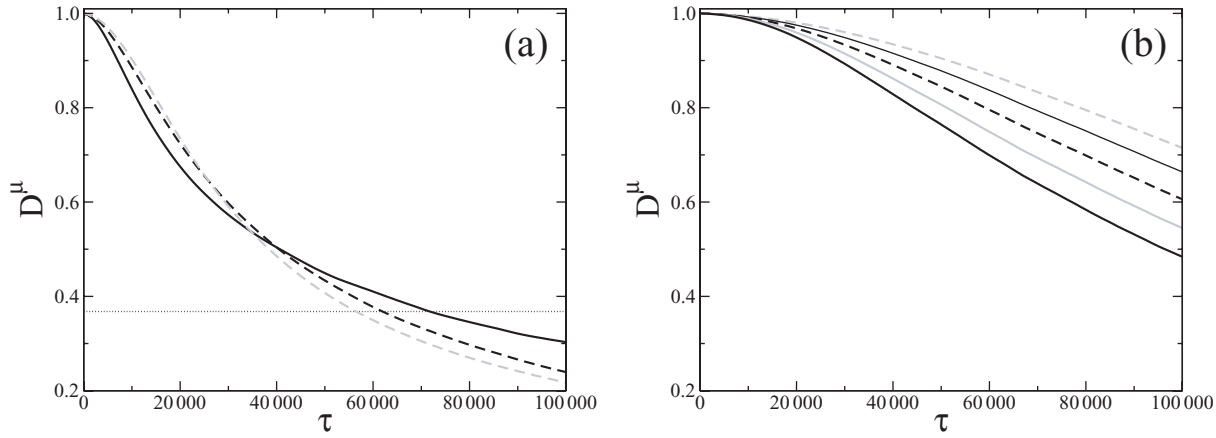

Figure 6. Effect of $1/f$ correlated noise extending in $[\gamma_m, \gamma_M] = [10^0, 10^9]\,s^{-1}$ for weak noise amplitude $\sigma < g = 0.1$ and different values of μ. The dashed gray curve refers to $\mu = 0$, the dashed black to $\mu = 0.50$, the thick black to $\mu = 1.00$. (a) Dephasing factor: correlations slightly increase dephasing at initial times and decrease it at longer times. The dotted horizontal line refers to e^{-1}. (b) Effect of a recalibration protocol: increasing the correlation coefficient increases dephasing. Thin black line corresponds to $\mu = 0.25$, thick gray to $\mu = 0.75$.

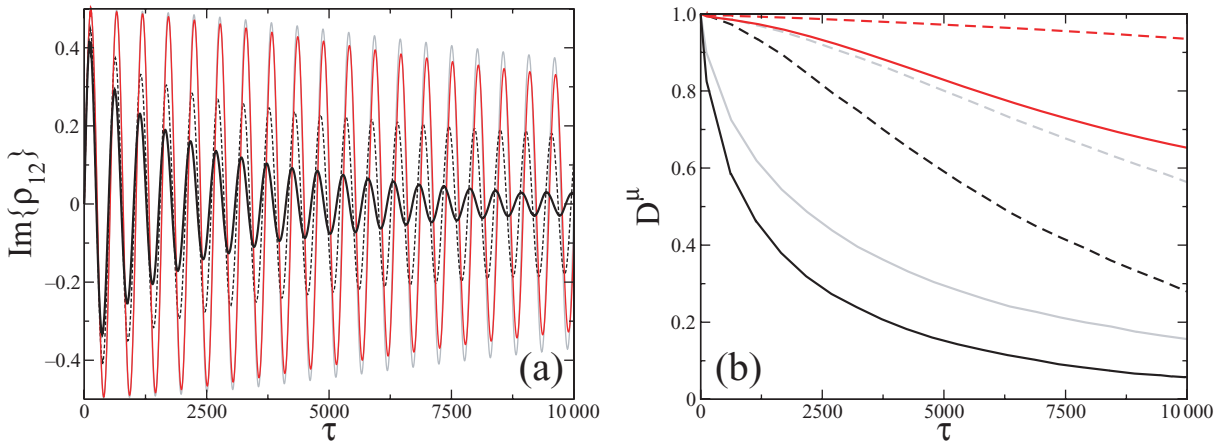

Figure 7. Effect of $1/f$ correlated noise extending in $[\gamma_m, \gamma_M] = [10^0, 10^9]\,s^{-1}$ for strong noise amplitude $\sigma > g = 0.01$ and different values of μ. (a) Dephasing factor for $\mu = 0$: black curves (dotted black for slow noise, solid black for low- and high-frequency noise); $\mu = 1$: gray (slow noise) and red (slow plus high-frequency noise). (b) The effect of a recalibration protocol is shown by the dashed curves, $\mu = 0$ black, $\mu = 0.75$ gray, $\mu = 1$ red. In both protocols (a) and (b) increasing the correlation coefficient decreases dephasing.

In single-qubit gates, the inhomogeneous broadening effect may be sensibly reduced by a recalibration protocol resetting the initial value of the system polarization at each run of the measurement protocol [9]. Recalibration turns out to be effective on two-qubit gates also in the presence of correlations among the noise sources. Results shown in figures 6(b) and 7(b) have

been obtained numerically by resetting the values of $x_\alpha(0)$ at each realization of the stochastic processes $x_\alpha(t)$. Interestingly, even if the effect of low-frequency components is practically eliminated by the recalibration procedure, the decay has a different dependence on μ depending on σ. In particular, if $\sigma < g$ the larger the correlation coefficient, the faster the signal decays (figure 6(b)), if instead $\sigma > g$ stronger correlations correspond to slower decay (figure 7(b)).

6. Conclusions

In the present paper, we have introduced a phenomenological model for $1/f$ correlated noise affecting a two-qubit gate in a fixed coupling scheme. Our analysis is based on analytical results obtained within the adiabatic approximation and on the numerical solution of the stochastic Schrödinger equation.

Due to the nonmonotonicity of the renormalized splitting in the SWAP subspace, the entangled dynamics sensitively depends on the ratio σ/g between the amplitude of the low-frequency noise and the qubit coupling strength. For small amplitude noise, correlations increase dephasing at the relevant short time scales (smaller than the dephasing time). On the other hand, under strong amplitude noise, an increasing degree of correlations between noise sources acting on the two qubits always leads to reduced dephasing. Our numerical analysis has shown that the above features hold true for adiabatic $1/f$ noise extending up to frequencies $10^9\ \mathrm{s}^{-1}$ about two orders of magnitudes smaller that the qubit Bohr frequencies.

We remark that the above results on the reduced dynamics in the SWAP subspace apply also to different two-qubit gates involving the same states, at least as long as the adiabatic approximation holds true. The performance of two-qubit gates involving states of the Z subspace, like the c-NOT gate, might be reduced in view of the larger sensitivity of the Z subspace to low-frequency charge noise [28].

We have analyzed the possibility of reducing the effects of low-frequency correlated noise by a open-loop recalibration protocol of the two-qubit gate. Despite counteracting the inhomogeneous broadening effect, the efficiency of the protocol still depends on the value of σ/g, the maximum efficiency occurring for small-amplitude uncorrelated noise ($\sigma < g$ and $\mu = 0$), or for strong-amplitude correlated noise ($\sigma > g$ and $\mu = 1$).

The observed reduced sensitivity of the SWAP subspace to correlated strong-amplitude noise might suggest exploiting this subspace to reliably encode a single qubit, in the same spirit as decoherence free subspaces (DFS) [32]. The possibility of avoiding errors due to correlated noise by encoding in DFS has indeed been recently discussed for superconducting qubits in [23, 33, 34]. This strategy rigorously applies to the pure dephasing regime where a DFS subspace exists for collective noise. In the situation analyzed in the present article, however, the SWAP subspace is not rigorously a DFS. In fact, in the presence of collective noise ($\mu = 1$), the interaction Hamiltonian (23) reads $-\frac{1}{2}(\sigma_1^{(1)} \otimes \mathbb{I}^{(2)} + \mathbb{I}^{(1)} \otimes \sigma_1^{(2)})\tilde{X}$. The system operator entering this coupling term has two degenerate eigenstates which do not span the SWAP subspace. In addition, for finite values of g, the system Hamiltonian (22) does not leave invariant the subspace spanned by the degenerate eigenstates, as DFS should require [35].

Acknowledgments

We thank Giuliano Benenti for his useful discussions. We acknowledge support from the EU-EuroSQIP (IST-3-015708-IP) and MIUR-PRIN2005 (2005022977).

Appendix. Moments entering $\sigma_{\delta\omega_{12}}$

From (28), it comes out that the marginal probability density function of x_α is a Gaussian function with standard deviation σ and zero average value. Then,

$$\langle x_\alpha^{2n}\rangle = \frac{(2n)!}{2^n n!}\sigma^{2n} \qquad \text{and} \qquad \langle x_\alpha^{2n+1}\rangle = 0, \tag{A.1}$$

(see [36]). Evaluation of the variance of the splitting fluctuations $\sigma_{\delta\omega_{12}}$ requires knowledge of the following mixed moments:

$$\begin{aligned}
\langle x_1^2 x_2^2\rangle &= \sigma^4(1+2\mu^2),\\
\langle x_1^2 x_2^4\rangle &= 3\sigma^6(1+4\mu^2),\\
\langle x_1^2 x_2^6\rangle &= 15\sigma^8(1+6\mu^2),\\
\langle x_1^4 x_2^4\rangle &= \sigma^8(9+72\mu^2+24\mu^4)
\end{aligned} \tag{A.2}$$

which directly follow from (13) by using (A.1).

References

[1] Zorin A B, Ahlers F-J, Niemeyer J, Weimann T and Wolf H 1996 *Phys. Rev.* B **53** 13682
[2] Nakamura Y, Pashkin Yu A and Tsai J S 1999 *Nature* **398** 786
[3] Vion D, Aassime A, Cottet A, Joyez P, Pothier H, Urbina C, Esteve D and Devoret M H 2002 *Science* **296** 886
[4] Petta J R, Johnson A C, Taylor J M, Laird E A, Yacoby A, Lukin M D, Marcus C M, Hanson M P and Gossard A C 2005 *Science* **309** 2180
[5] Weissman M B 1988 *Rev. Mod. Phys.* **60** 537
[6] Duty T, Gunnarsson D, Bladh K and Delsing P 2004 *Phys. Rev.* B **69** 140503
[7] Simmonds R W, Lang K M, Hite D A, Nam S, Pappas D P and Martinis J M 2004 *Phys. Rev. Lett.* **93** 077003
Cooper K B, Steffen M, McDermott R, Simmonds R W, Oh S, Hite D A, Pappas D P and Martinis J M 2004 *Phys. Rev. Lett.* **93** 180401
[8] Lisenfeld J, Lukashenko A, Ansmann M, Martinis J M and Ustinov A V 2007 *Phys. Rev. Lett.* **99** 170504
[9] Falci G, D'Arrigo A, Mastellone A and Paladino E 2005 *Phys. Rev. Lett.* **94** 167002
[10] Paladino E, Faoro L, Falci G and Fazio R 2002 *Phys. Rev. Lett.* **89** 228304
[11] Slichter C P 1996 *Principles of Magnetic Resonance* (Berlin: Springer)
[12] Ithier G *et al* 2005 *Phys. Rev.* B **72** 134519
[13] Nakamura Y, Pashkin Yu A, Yamamoto T and Tsai J S 2002 *Phys. Rev. Lett.* **88** 047901
[14] Falci G, D'Arrigo A, Mastellone A and Paladino E 2004 *Phys. Rev.* A **70** 040101
[15] Rigetti C, Blais A and Devoret M 2005 *Phys. Rev. Lett.* **94** 240502
Averin D V and Bruder C 2003 *Phys. Rev. Lett.* **91** 57003
Plastina F and Falci G 2003 *Phys. Rev.* B **67** 224514
Majer J *et al* 2007 *Nature* **449** 443
[16] Yamamoto T, Pashkin Y A, Astafiev O, Nakamura Y and Tsai J S 2003 *Nature* **425** 941
[17] Pashkin Y A, Yamamoto T, Astafiev O, Nakamura Y, Averin D V and Tsai J S 2003 *Nature* **421** 823
[18] Plantenberg J H, de Groot P C, Harmans C J P M and Mooij J E 2007 *Nature* **447** 836
[19] Governale M, Grifoni M and Schön G 2001 *Chem. Phys.* **268** 273
Thorwart M and Hänggi P 2002 *Phys. Rev.* A **65** 012309
Storcz M J and Wilhelm F K 2003 *Phys. Rev.* A **67** 042319
[20] Zimmerli G, Eiles T M, Kauz R L and Martinis J 1992 *Appl. Phys. Lett.* **61** 237
[21] Hu Y, Zhou Z-W, Cai J-M and Guo G-C 2007 *Phys. Rev.* A **75** 052327

[22] Vion D 2007 private communication
[23] Papoulis A 1965 *Probability, Random Variables and Stochastic Processes* (New York: McGraw Hill)
[24] You J Q, Hu X and Nori F 2005 *Phys. Rev.* B **72** 144529
[25] Astafiev *et al* 2004 *Phys. Rev. Lett.* **93** 267007
[26] Bendat J S and Piersol A G 1993 *Engineering Applications of Correlation and Spectral Analysis* 2nd edn (New York: Wiley-Interscience)
[27] Mastellone A, D'Arrigo A, Paladino E and Falci G in preparation
[28] Mastellone A, D'Arrigo A, Paladino E and Falci G 2008 *Eur. Phys. J.—Spec. Top.* **160** 291
[29] Landau R H and Pèz M J 1997 *Computational Physics, Problem Solving With Computers* (New York: Wiley-Interscience)
[30] Nielsen M A and Chuang I L 2000 *Quantum Computation and Quantum Information* (Cambridge: Cambridge University Press)
[31] Benenti G, Casati G and Strini G 2007 *Principles of Quantum Computation and Information* vol 2 (Singapore: World Scientific)
[32] Zanardi P and Rasetti M 1998 *Phys. Rev. Lett.* **79** 3306
[33] Zhou X, Wulf M, Zhou Z, Guo G and Feldman M J 2004 *Phys. Rev.* A **69** 030301
[34] Storcz M J, Vala J, Brown K R, Kempe J, Wilhelm F K and Whaley K B 2005 *Phys. Rev.* B **72** 064511
[35] Lidar D A and Whaley K B 2003 *Irreversible Quantum Dynamics* (*Springer Lecture Notes in Physics* vol 622) ed F Benatti and R Floreanini (Berlin: Springer)
[36] Gardiner C W 1996 *Handbook of Stochastic Methods: For Physics, Chemistry, and the Natural Sciences* 2nd edn (Berlin: Springer)